Single-Crystal Growth of Gum Metal and its Elasticity

Yusuke SHIMIZU*, Takeshi YANO, and Naohisa TAKESUE

(Received May 31, 2008)

Abstract

Single crystals of Gum Metal (Ti-based multinary alloy Ti-Nb-Ta-Zr-O) have been grown successfully in an Ar gas flow by a floating zone method. The growth orientations were determined approximately by using seed crystals with the desired orientations. The various growth conditions were realized by choosing the gas purity, the gas flow rate, and the growth rate as variables. Composition analysis of the grown crystals were done to check any variation from the values of the raw material along with the bulk homogeneity, followed by measurements of the lattice parameter and the hardness, which provides the following results: (1) The composition of oxygen varies with respect to the flow rate, or is increased as the purity is degraded, (2) The lattice parameter is increased with increasing of the composition, (3) which is also the case with the hardness. Measurements of the elastic constants and Young's moduli were performed to investigate the elasticity. The results indicate that the crystals exhibit the anisotropy which was expected previously.

Key words: solid solutions, single crystal growth, alloys, elasticity

1. Introduction

Gum Metal belongs to a class of β-type titanium alloys and typically has the concentration Ti-36Nb-2Ta-3Zr-0.3O in mass%. This alloy obtained after significant cold swaging is known to exhibit excellent mechanical multifunctionality at room temperature such as non-linear ultra-low elasticity, ultra-high strength, and superplastic-like workability [1-3]. Out of these properties, we focus on the unique plasticity that the deformation occurs at tensile stress near the ideal strength [3]. The uniqueness suggests that the process requires no movement of dislocations, and this type of deformation is likely to supply the superiority which causes no work hardening.

In general, metals and alloys do not undergo the ideal deformation since the ideal strength is usually 20-30 times higher than the threshold for slips of dislocations. In order to cause the dislocation-free process, this tendency must be reversed. The requirement can be satisfied by chemical alloy designing to sufficiently reduce the ideal stress [4,5], along with the preliminary cold working to elevate the threshold as mentioned above.

* Department of Applied Physics, Graduate School of Science, Fukuoka University, 8-19-1 Nanakuma, Jonan-ku, Fukuoka 814-0180, Japan
E-mail: sd071003@cis.fukuoka-u.ac.jp

For the bcc systems, the ideal shear stress makes sense regarding the intrinsic slip directions ⟨111⟩ , and has the following relationship with the shear modulus of the ⟨111⟩ directions [5,6],

$$\tau_{max} \cong 0.11 G_{111},$$

where τ_{max} and G_{111} are the ideal shear stress and the shear modulus, respectively. Since using elastic constants in the cubic system G_{111} is expressed as,

$$G_{111} = \frac{3c_{44}(c_{11} - c_{12})}{c_{11} - c_{12} + 4c_{44}} .$$

τ_{max} is apparently proportional to $(c_{11} - c_{12})$ [3,5-7]. This difference must be small to realize the ideal deformation, which leads to concurrence of a small Young's modulus for the ⟨100⟩ directions as given by [3-7],

$$E_{100} = \frac{(c_{11} - c_{12})(c_{11} + 2c_{12})}{c_{11} + c_{12}} ,$$

where E_{100} is the one for the direction. Results of first-principle calculation previously done [4,5] expected that the alloy exhibits this elastic anisotropy so that the ideal process is possible. This expectation must be proved experimentally, and the direct verification through experiments requires the single-crystal specimens. This situation motivated us to perform technical try of the growth which was followed by characterization of the crystals and measurements of the elastic constants and Young's moduli; they were basically done at room temperature.

2. Experimentals

Polycrystalline rods of the raw material were used for growth of the crystals. They were obtained through several steps consisting of the preparatory processes such as billet forming from mixed powders of the constituents, sintering, hot forging, cold machining. Details of the entire preparation are written in Ref. 7. The composition after the final step was determined by x-ray fluorescence analysis for the metal components, Nb, Ta, and Zr, and the rest O by a combustion method. The results showed no significant change from the typical concentration.

A floating zone furnace (four-mirror type, FZ-T-4000-H, Crystal Systems Inc.) was used to grow the crystals [7]. The growth was carried out in a steady flow of an Ar gas at a fixed growth rate. To establish the various growth conditions, the gas purity, the flow rate, and the growth rate were employed as the variables. Conditioning was done in choice of their values such as the purity of either 99.99% or 99.9999%, the flow rate of 0.5-10 L/min (L means liter hereafter), and the growth rate of 1-10 mm/min. In many cases of the try, the growth orientation was controlled by using the preliminary-grown seed crystals, which enabled us to obtain the crystals grown approximately along the ⟨100⟩, ⟨110⟩, ⟨111⟩ directions. The grown crystal was solution treated at 1373 K for 30 min in an Ar-sealed quartz tube, and was subsequently quenched into water. The composition was analyzed by the same methods as those used for the polycrystalline rods. The crystal quality was inspected by x-ray diffraction, and the growth direction and the lattice parameters were then determined to investigate any variation with respect to the growth condition. Additionally, the Vickers hardness was measured at 10 kg loading on the same purpose.

Measurements of the elastic constants were done by a piezo-induced-ultrasonic cubic resonant method (Nihon Techno-Plus Inc. CC-RT) [7, 8-10]. This method requires the rectangular parallelepiped single

crystal whose faces are all {100} planes. Such specimens whose sides are 2 to 4 mm were cut from the grown crystal, followed by mechanical polishing, so that a surface normal of each face is approximately along the ⟨100⟩ direction. The specimens were reused for compression tests (Shimadzu AG-50KNI) [7] for quick survey of the deformation behavior as well as obtaining Young's modulus of the ⟨100⟩ direction.

Tensile tests (also Shimadzu AG-50KNI) [7] were performed to measure Young's modulus along again the ⟨100⟩ direction to double check with the data given by the compression, and the moduli also along the ⟨110⟩ and ⟨111⟩ directions to find any anisotropy. To obtain the specimens, the crystals grown along the three directions were machined to be shaped rod-like, and were each provided for the measurements along the corresponding direction.

3. Results and discussion

Results of the x-ray diffraction indicated that the growth rate, one of the three variables, has a substantial effect on only the crystal quality. The intensity distribution of the Bragg reflections showed that all bulks grown at the employed growth rate are almost entirely single crystals, but that the growth performed at the higher rate provides the higher mosaicity. Since this tendency becomes significant beyond the rate of 6mm/hr, this value allows the most efficient performance which gives the quality excellent enough to accomplish the planned measurements, and was thereafter employed universally in many cases to obtain the specimens. Fig. 1 shows a picture of the typical crystal whose shape is cylindrical; the diameter is about 6mm, and the length is about 65mm. The furnace provides the crystal with the optional size, but because of the performance limit, the diameter employed is usually 6-9mm, and the length shorter than 130mm.

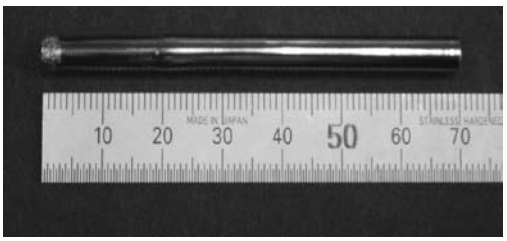

Fig. 1. A picture of the typical grown crystal.

On the other hand, results of the composition analysis implied that the other two variables, the purity and the flow rate, have remarkable effects on the oxygen concentration. Dependence of the concentration on the flow rate [7] is given in Fig. 2. The data were obtained by using the gas with the purity 99.99%. The figure shows that the concentration is increased with increasing of the flow rate. This dependence implies that increase of the concentration is caused by the impurity contained in the gas used. The extra solutionized oxygen elevated the hardness as presented in the same figure. This effect corresponds to the solution hardening which leads us to learn importance of the concentration. The oxygen also gave rise to increase of the lattice parameter [7] as shown in Fig. 3. This tendency is what is usually observed.

Using the other gas with the higher purity 99.9999% significantly prevented increase of the oxygen concentration. Results of the chemical analysis indicated that the growth with the flow at 4-10L/min makes only the trivial difference from the prepared oxygen concentration. All results obtained throughout the analysis provide us the growth conditions so that the oxygen concentration can be controlled in

terms of the two variables.

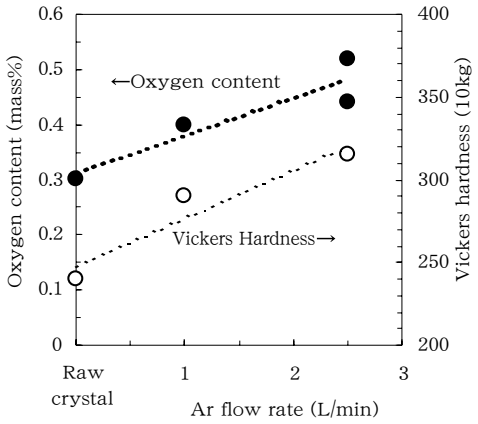

Fig. 2. Dependence of the oxygen concentration and the hardness on the flow rate.

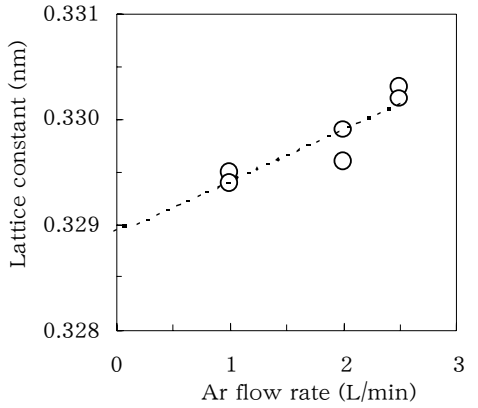

Fig. 3. Dependence of the lattice parameter on the flow rate.

The other elements, Nb, Zr, and Ta exhibit their concentration gradients with respect to the length of the grown crystals [7] as shown in Fig. 4. The non-zero slopes mean the initial transient stage of the growth during which the solute diffusion is under its unsteady state. The plots in the figure suggest that the growth length of less than about 25 mm is a trace of the unsteady solidification. Beyond the initial portion the concentrations approach those of the nominal values giving the zero slopes, implying that the steady state is achieved. Signs of the gradients, positive or negative, are determined depending on values of the equilibrium distribution coefficients of the three elements to Ti. If the value is greater than unity, the slope is negative, which is the case with Nb and Ta, and oxygen was also found to be involved in this case. Otherwise, positive the case with Zr. The unsteady portions including the unwanted chemistry were removed by cutting off from the main bulk crystal before the subsequent solution treatment.

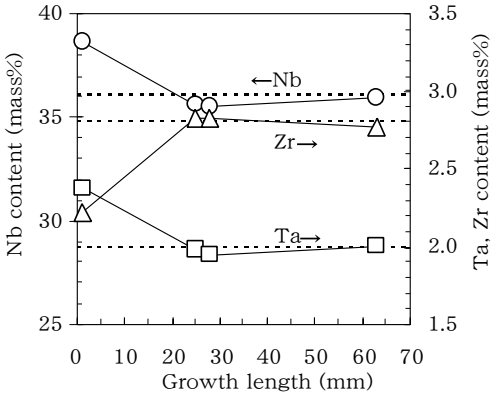

Fig. 4. Concentration gradients of Nb, Zr, Ta with respect to the length.

Values of the elastic constants c_{11}, c_{12}, c_{44} experimentally determined are 135.1, 122.0, 15.3 GPa, respectively [7]. A size of the specimen for this measurement is 2.1×2.4×2.4 mm^3 and the composition is Ti-35.4Nb-1.9Ta-2.8Zr-0.37O in mass%. The obtained data were used for analysis of the elastic anisotropy after describing results of the compression and tensile tests below.

Fig. 5 shows a typical stress-strain curve obtained from the repeated compression test along the ⟨100⟩ direction [7]. The specimen size for this measurement is 2.8×3.5×3.8 mm^3 and the composition is Ti-

35.9mass%Nb-2.0Ta-2.8Zr-0.30O in mass%. The curve exhibits quite normal behavior of the deformation, and provides E_{100} about 36 GPa.

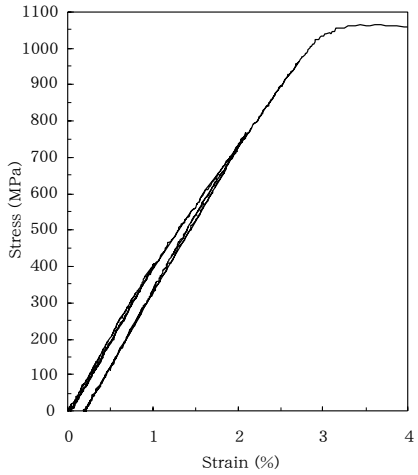

Fig. 5. A stress-strain curve obtained from the repeated compression test along the ⟨100⟩ direction.

Fig. 6 (a)-(c) are the stress-strain curves given by the repeated tensile test along the ⟨100⟩, ⟨110⟩, and ⟨111⟩ directions, respectively. The compositions of the specimens in mass% are correspondingly Ti-36.1Nb-2.0Ta-2.78Zr-0.49O, Ti-36.7Nb-2.07Ta-2.7Zr-0.30O, and Ti-35.2Nb -1.84Ta -2.91Zr-0.32O in mass%. The figures give us values of three Young's moduli $E_{100}\sim$ 40 GPa, $E_{100}\sim$ 60 GPa, and $E_{111}\sim$ 86 GPa; the value of E_{100} is close to the one obtained from the compression. The three values are apparently different each other, implying the elastic anisotropy expected.

The anisotropy can be inspected through calculating the modulus for an arbitrary direction ⟨xyz⟩ in terms of the elastic constants according to the following equation [11],

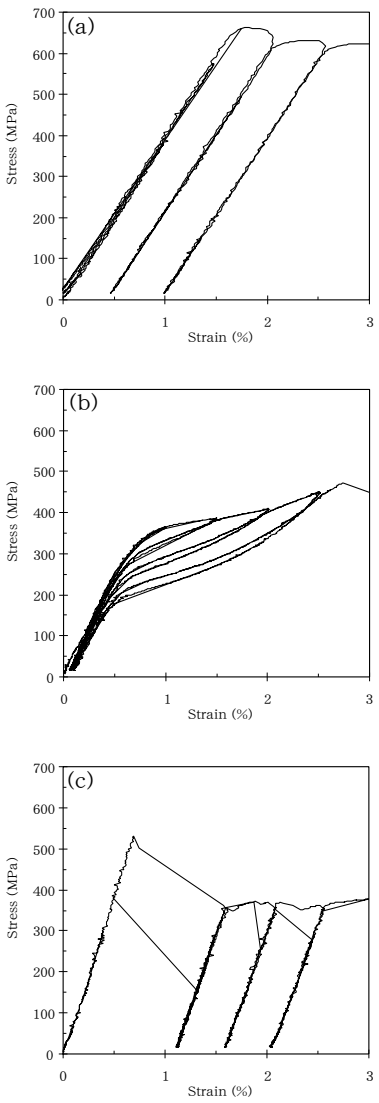

Fig. 6. Stress-strain curves given by the repeated tensile test along (a) the ⟨100⟩, (b) ⟨110⟩, and (c) ⟨111⟩ directions.

$$E_{xyz}=\left\{\frac{c_{11}+c_{12}}{(c_{11}-c_{12})(c_{11}+2c_{12})}+\left(\frac{1}{c_{44}}-\frac{2}{c_{11}-c_{12}}\right)(l^2m^2+m^2n^2+n^2l^2)\right\}^{-1},$$

where l, m, n are direction cosines of the [xyz] direction with the three ⟨100⟩ directions, respectively. A result of the calculation is given as a solid line in Fig. 7

representing variation of E_{xyz} with respect to the [xyz] direction on the (0$\bar{1}$1) plane, where the direction is denoted by θ which is the angle from the [100] direction. The measured three moduli are shown in the figure by solid circles. The curve drawn in the figure also implies the anisotropy clearly, but lies way below the measured data points, indicating almost half the values. It is normal to think that the difference comes from inaccuracy of the elastic constants, since the determination requires quite precise shape geometry of the specimen such as high parallelity and orthogonality among the faces which are very difficult to realize.

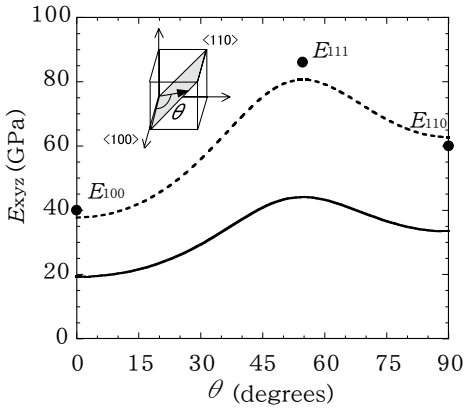

Fig. 7. Young's modulus with respect to the [xyz] direction on the (0$\bar{1}$1) plane.

By using the elastic constants as adjustable parameters, the curve of E_{xyz} were modified so that the curve goes through the three points. The modified curve is also given as a broken line in Fig. 7, indicating good matching with the data points. This way does not determine values of c_{11}, c_{12}, c_{44} independently because the equations of E_{100}, E_{110}, E_{111} have ($c_{11}-c_{12}$) as their common product term, but this term itself and c_{44} could be determined, and the subtle nonlinear fitting provides quite uniquely $c_{11}-c_{12}\sim$ 25 GPa and $c_{44}\sim$ 30 GPa, which leads to the elastic anisotropy factor $(c_{11}-c_{12})/2c_{44}\sim$ 0.42 implying the anisotropy consistently.

The specimens used for all tests had the various oxygen concentrations different each other. Plots of all obtained Young's moduli, strengths, elongations with respect to the concentration are given in Fig. 8 (a)-(c), where the figure (b) and (c) do not contain the plots relevant to the ⟨100⟩ tests for lack of data. The figure (a) shows that Young's moduli do not vary with respect to the concentration. On the other hand, the figure (b) indicates that the strengths are increased as the concentration is increased, and the figure (c) presents the reverse effect. The latter two tendencies were the same as those previously observed in the polycrystalline specimens [12]. The features obtained from Fig. 8 provide us ideas to control the mechanical properties in terms of the growth conditions, i.e., the gas purity and its flow rate.

The stress-strain curve obtained from the test along the ⟨110⟩ direction, given in Fig. 6 (b), is remarkably different from the other two curves, and obviously shows nonlinear elastic response and hysteresis loops, suggesting a martensitic transformation, likely β-to-α", where α" means the martensitic phase whose structure is orthorhombic [13, 14] or monoclinic. This possible pseudoelastic behavior may be a main cause of the nonlinear elasticity which only the polycrystalline material has been thought to exhibit. The expectation has not been proved at this moment. The further investigation is ongoing.

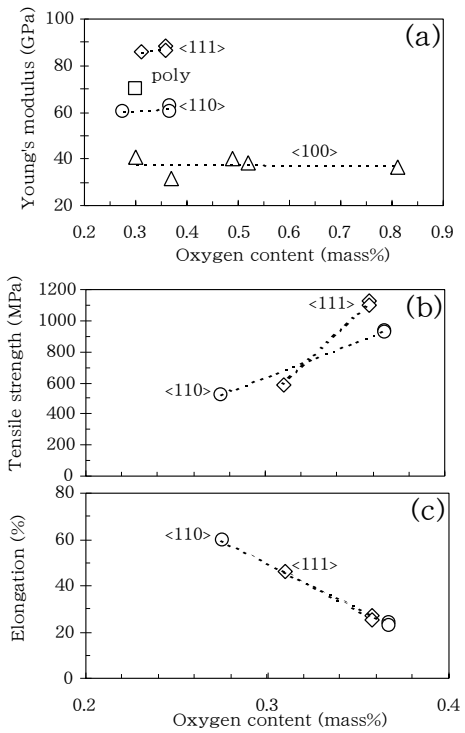

Fig. 8. All obtained (a) Young's moduli, (b) strengths, (c) elongations with respect to the concentration.

4. Conclusion

A method of single-crystal growth of Gum Metal has been established. The growth orientations, the crystal quality, and the oxygen concentration can be controlled in terms of the three variables, that is, the growth rate, the gas purity, and its flow rate. Young's moduli obtained from the compression tests along the ⟨100⟩ direction and the tensile tests along the ⟨100⟩, ⟨110⟩, ⟨111⟩ directions showed the elastic anisotropy as expected. The moduli were found to exhibit no dependence on the oxygen concentration. On the other hand, the strengths and the elongations also obtained from the same tests indicate their significant dependence; the higher strengths, the higher concentration, and the reverse is true for the elongations. An origin of the nonlinear elasticity of Gum Metal may be related to the response of the grown crystal exhibited to loading along the ⟨110⟩ direction. The obtained hysteresis loops suggests the martensitic transformation to the α'' phase.

Acknowledgment

This work was supported by Toyota R&D Lab. collaborative research program, and partially by the Kurata Memorial Hitachi Science and Technology Foundation.

References

[1] T. Saito, T. Furuta, J. H. Hwang, S. Kuramoto, K. Nishino, N. Suzuki, R. Chen, A. Yamada, K. Ito, Y. Seno, T. Nonaka, H. Ikehata, N. Nagasako, C. Iwamoto, Y. Ikuhara, T. Sakuma, Science 300 (2003) 464.

[2] T. Furuta, K. Nishino, J. H. Hwang, A. Yamada, K. Ito, S. Osawa, S. Kuramoto, N. Suzuki, R. Chen, T. Saito, Ti-2003 Science and Technology, G. Lütjering and J. Albrecht (Eds.) WILEY-VCH Weinheim (2004) 1519.

[3] S. Kuramoto, T. Furuta, J. H. Hwang, Y. Seno, T. Nonaka, H. Ikehata, N. Nagasako, K. Nishino, T. Saito, C. Iwamoto, Y. Ikuhara, T. Sakuma, Ti-2003 Science and Technology, G. Lütjering and J. Albrecht (Eds.) WILEY-VCH Weinheim (2004) 1527.

[4] H. Ikehata, N. Nagasako, T. Furuta, A. Fukumoto, K. Miwa, T. Saito, Phys. Rev. B 70 (2004) 174113.

[5] T. Li, J. W. Morris Jr., N. Nagasako, S. Kuramoto, D. C. Chrzan, Phys. Rev. Lett. 98 (2007) 105503.

[6] C. R. Krenn, D. Roundy, J. W. Morris

Jr., M. L. Cohen, Materials Science and Engineering A319-321 (2001) 111.
[7] M. Hara, S. Kuramoto, N. Takesue, Ti-2007 Science and Technology, M. Niinomi et al. (Eds.) N.K.G. Japan (2007) 627.
[8] K. Tanaka, Materia Japan 35 (1996) 380.
[9] K. Tanaka and M. Koiwa, Materia Japan 36 (1997) 254.
[10] K. Tanaka and M. Koiwa, Kinzoku 69 (1999) 129.
[11] J. J. Wortman and R. A. Evans, J. of Appl. Phys. 36 (1965) 153.
[12] T. Furuta, S. Kuramoto, R. Chen, J. H. Hwang, K. Nishino, T. Saito, J. Japan Inst. Metals 70 (2006) 579.
[13] S. Kuramoto, K. Nishino, T. Saito, J. of Japan Inst. Light Metals 55 (2005) 618.
[14] T. Furuta, S. Kuramoto, J. H. Hwang, K. Nishino, T. Saito, M. Niinomi, Materials Transactions 48 (2007) 1124.